

# Journal of Materials Chemistry C

# A pyrimidine end-capped electron transport material interacted with silver improving electron-injection and long-term stability in OLED

Journal:	Journal of Materials Chemistry C	
Manuscript ID	TC-ART-08-2024-003534.R1	
Article Type:	Paper	
Date Submitted by the Author:	01-Oct-2024	
Complete List of Authors:	Chen, Yuhui; Yamagata Daigaku, Organic Device Engineering Sano, Takeshi; Yamagata University, FROM Sasabe, Hisahiro; Yamagata univ., Organic Device Engineering Sugiyama, Ryo; Yamagata univ., Organic Device Engineering Matsunaga, Amane; Yamagata Daigaku, Organic Materials Science Sato, Hiroki; Yamagata Daigaku, Organic Materials Science Katagiri, Hiroshi; Yamagata University, Graduate School of Science and Engineering Kido, Junji; Yamagata Daigaku, Organic Materials Science	

SCHOLARONE™ Manuscripts A pyrimidine end-capped electron transport material interacted with silver improving electron-injection and long-term stability in OLED

Yuhui Chen [a], Takeshi Sano\*[b], Hisahiro Sasabe\*[a], [c], [d], Ryo Sugiyama [a], Amane Matsunaga [a], Hiroki Sato [a], Hiroshi Katagiri [a], [c], [d], and Junji Kido\*[a], [b], [c], [d]

- [a] Department of Organic Materials Science, Yamagata University, 4-3-16 Jonan, Yonezawa, Yamagata, 992-8510, Japan
- [b] Innovation Center for Organic Electronics (INOEL), Yamagata University, 1-808-48 Arcadia, Yonezawa, Yamagata, 992-0119, Japan
- [c] Research Center for Organic Electronics (ROEL), Yamagata University, 4-3-16 Jonan, Yonezawa, Yamagata 992-8510, Japan
- [d] Frontier Center for Organic Materials (FROM), Yamagata University, 4-3-16 Jonan, Yonezawa, Yamagata, 992-8510, Japan

E-mail: <u>takeshi.sano@yz.yamagata-u.ac.jp</u>, <u>h-sasabe@yz.yamagata-u.ac.jp</u>, <u>kid@yz.yamagata-u.ac.jp</u>

Keywords: organic semiconductor; electron-transport material; electron-injection material; pyrimidine; metal complexation

# **Abstract**

Although organic light-emitting devices (OLEDs) have been commercialized for display applications, electron-injection layers (EILs) still relied on alkali metals or their compounds to lower driving voltages, and hence reactivity with atmospheric moisture is a primary concern, especially in flexible devices. As an alternative strategy, combining electron transport materials (ETMs) based on 1,10-phenanthroline (Phen) derivatives with silver (Phen/Ag) has attracted much attention for developing air-stable EILs. However, most studies have focused on Phen derivatives. Herein, we developed a non-Phen ETM named **DPmPy-BP** based on 2,6-di(pyrimidin-2-yl) pyridine skeleton. Combined with Ag (**DPmPy-BP**/Ag) as a potentially air-stable EIL, this ETM exhibited superior electron-injection properties and remarkable stability in preliminary green phosphorescent OLEDs achieving a maximum external quantum efficiency (EQE) of 20% and an operational lifetime (LT<sub>50</sub>) of approximately 17,000 hours at 1000 cd m<sup>-2</sup>, which surpass those of **Phen/**Ag devices and are

comparable to devices using a conventional alkali metal compound 8-hydroxyquinolinolatolithium (**Liq**) as the EIL (**DPmPy-BP/Liq**).

#### 1. Introduction

Achieving better performance of organic light emitting diodes (OLEDs) requires low operating voltage technology to ensure lower electrical power consumption, longer lifetimes, and higher efficiency simultaneously. [1] For conventional OLEDs, a typical method to reduce the operating voltage is to modify the electron-injection barrier at cathode metal/electron transport material (ETM) interfaces using electron-injection layers (EILs) with low work function (WF) metals such as alkali metals, alkaline earth metals, and their compounds. [2-6] Since this conventional strategy would hamper operational stability of OLEDs due to their high reactivity and diffusivity, novel electron-injection methods that eliminate alkali metals have been attractive for both long-term stable OLEDs and further applications such as unencapsulated flexible devices. [7-10]

As one potent approach, the combinations of 1,10-phenanthroline (Phen) based ETMs and cathode metals (Ag, Al) were reported functionable as air-stable EILs. [11-16] To achieve broad generalizability in developing the aforementioned ETMs, Yoshida firstly pointed out the pivotal role of the Ag-bathocuproine (**BCP**) complex by using low energy inverse photoemission spectroscopy. [13] Afterwards, Duan's group developed a series of Phen derivatives by introducing various electron-donating moieties to investigate impacts on electron-injection doped with Ag. They concluded these combinations (Phen/Ag) act as n-doping EIL through coordination induced activation. [14] Fukagawa and coworkers suggested that the electron-injection effect could be enhanced by modifying Phen skeleton with strong electron-donating group such as alkoxy groups, and dialkylamino groups. [16] Despite these findings, most ETMs reported applicable as Ag-partners are still confined to Phen derivatives. [17-19] Inevitably, when applied as ETMs, Phen derivatives present several drawbacks, including low triplet energy ( $E_{\rm T}$ ), low glass-transition temperature ( $T_{\rm g}$ ) and limited synthetic variety. [6, 20, 21]

In this work, we developed a novel non-Phen ETM named 2,6-di(pyrimidin-2-yl)-4-([1,1'-biphenyl]-4-yl) pyridine (**DPmPy-BP**), also served as a potentially air-stable EIL combined with Ag (**Figure 1**). Notably, **DPmPy-BP** demonstrates much better electron-injection than 4'-([1,1'-biphenyl]-4-yl)-2,2':6',2"-terpyridine<sup>[22]</sup> (**TPy-BP**) when doped with

Ag, Moreover, **DPmPy-BP** exhibits both higher  $E_T$ , deeper ionization potential ( $I_p$ ), and better electron-injection combined with Ag compared to the typical Phen derivative **BCP**, simultaneously. A green phosphorescent OLED device using **DPmPy-BP** as both the ETL and hole-blocking layer (HBL), with Ag-doped **DPmPy-BP** as the EIL, successfully achieved a lower turn-on voltage than devices using **BCP/Liq** or **BCP/Ag**. The maximum external quantum efficiency (EQE) of 20% and an operational lifetime (LT<sub>50</sub>) of approximately 17,000 hours at 1000 cd m<sup>-2</sup> surpass those of **BCP/Ag** devices and are comparable to devices using **Liq** as the EIL (**DPmPy-BP/Liq**). Furthermore, the atmospheric stability was also significantly improved over devices using **Liq**, indicating its potential effectiveness as an air-stable EIL.

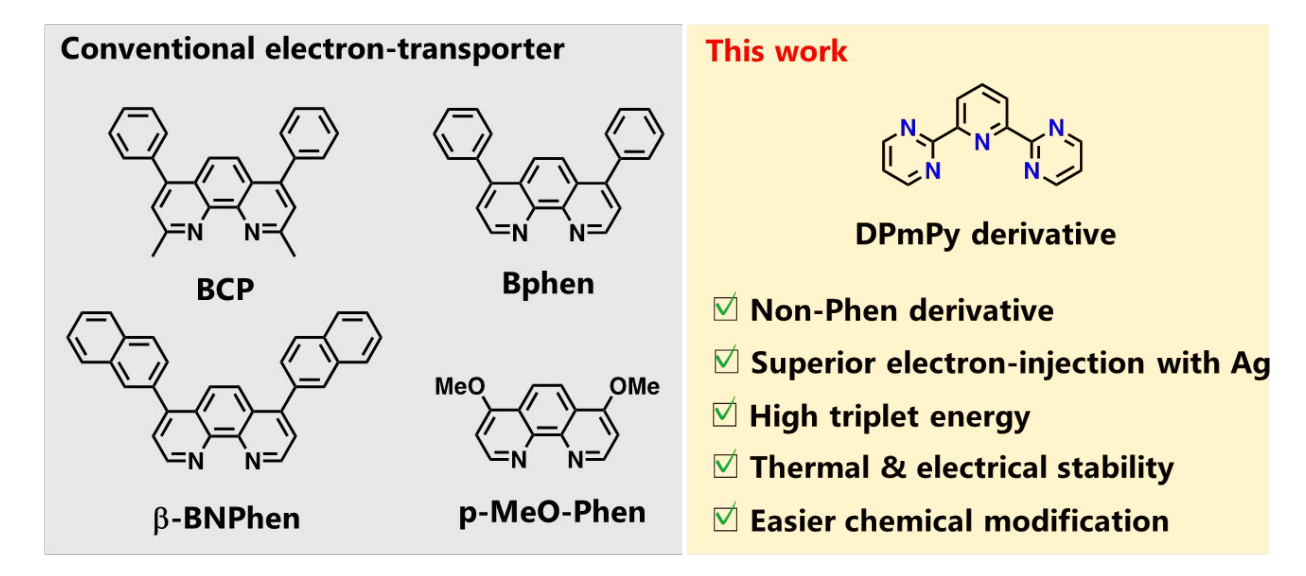


Figure 1. Concept of molecular design in this work

# 2. Results and Discussion

#### 2.1. Molecular design and electronic structure calculation

To find a replacement of Phen derivatives in terms of metal coordination, it is paramount to extract the unique characteristic from the Phen skeleton. Perceptibly, different from other typical bidentate ligands, the planar Phen skeleton has no conformational isomer because of the structural rigidity. On the other hand, while recognized as a classic tridentate chelating ligand for transition-metal ions, [23] 2,2':6',2"-terpyridine (**TPy**) moiety is a well-known component for ETMs owing to its intrinsic electron-accepting nature, thermal stability, high  $E_{\rm T}$ , as well as abundance in chemical modification. [24] However, several conformational isomers of **TPy** would be induced (**Figure 2**a). [24a, 25] This issue raises concerns regarding metal coordination when used in the solid-state. In this context, by replacing both two

peripheral pyridines in **TPy** with pyrimidines, conformational isomers could be reduced to enhance metal complexation with Ag (Figure 2a). As such, we designed **DPmPy-BP**, and compared it with **TPy-BP** (Figure 2b).

Prior to the synthesis of materials, to estimate the coordination ability as well as the optoelectronic properties, density functional theory (DFT) and time-dependent DFT (TD-DFT) calculations were conducted utilizing Gaussian09<sup>[26]</sup> with the B3LYP/6-31G(d) basis set. The optimized geometric structures, frontier molecular orbitals and electrostatic potential (ESP) maps are depicted in Figure 2. Both **TPy** and **DPmPy** exhibited quasi-planar geometries as the most stable conformation, where the twisted angles between peripheral and core rings were below 2° and 3°, respectively. However, for **TPy-BP**, neither peripheral pyridine rings rotated similarly to the isomer of **TPy-metal** complex because of steric strain and the formation of the intramolecular CH····N hydrogen bonds (H-bonds). To further clarify possible conformational isomers of **TPy-BP** and **DPmPy-BP**, potential energy surface (PES) scan was also performed (Figures S1-S2). In contrast with **TPy-BP**, the conformation isomers of **DPmPy-BP** were confirmed to be reduced as expected.

Consequently, the maximum ESP of **DPmPy-BP** was confirmed to localize around the nitrogen atoms in **DPmPy** unit while that of **TPy-BP** was close to each nitrogen atoms in terpyridine moiety. Thereby the maximum ESP of **DPmPy-BP**, which was -0.098, was about twice larger than that of **TPy-BP**. Such results indicated higher nucleophilicity and stronger intermolecular H-bonds as well as coordination ability with metals of **DPmPy-BP** comparing to **TPy-BP**. In addition, the highest occupied molecular orbital (HOMO) and the lowest unoccupied molecular orbital (LUMO) levels of **DPmPy-BP** were slightly deeper than those of **TPy-BP** due to increased electron-accepting abilities from the additional nitrogen atoms. The *E*<sub>T</sub> values were over 2.85 eV suggesting their possible applications to blue and green phosphorescent and/or thermally activated delayed fluorescent (TADF) OLEDs. Results of **BCP** were also compared (Figures S3-S4).

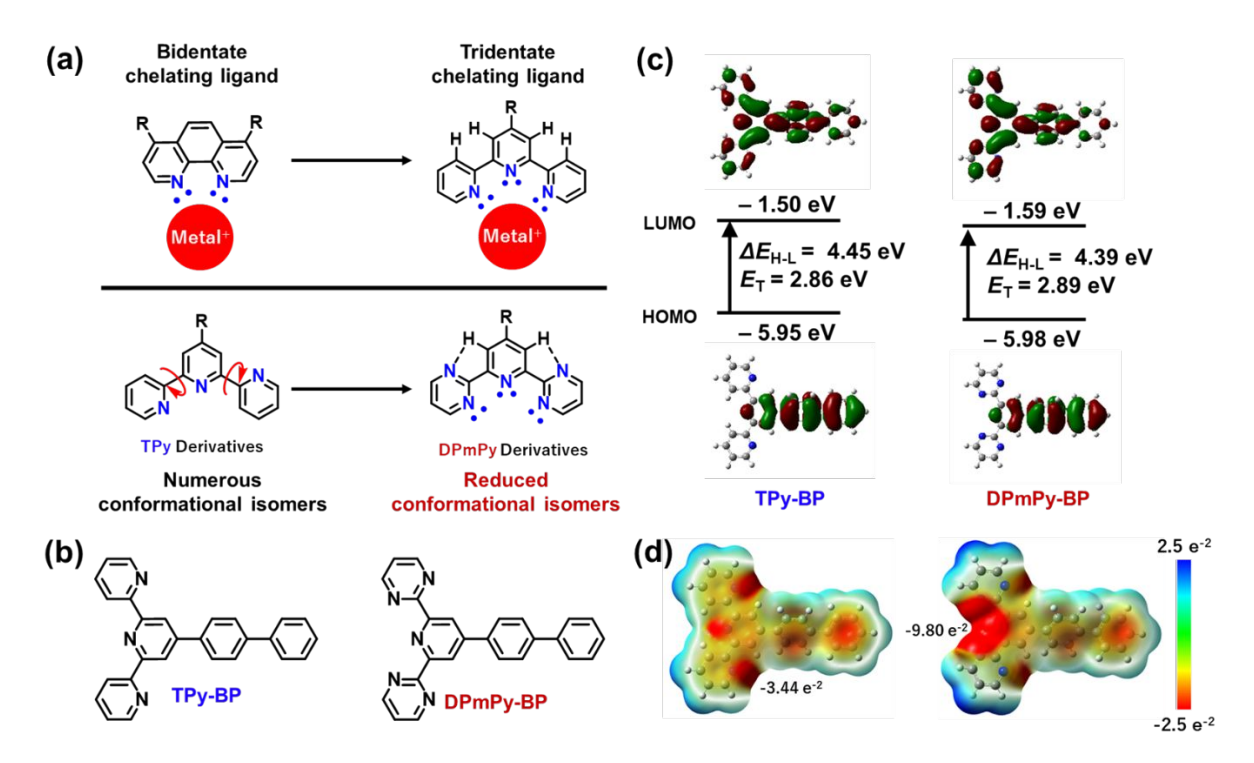


**Figure 2.** (a) The schematic illustration of molecular design. (b) Chemical structures of **TPy-BP** and **DPmPy-BP**. (c) HOMO and LUMO distributions and energy levels; HOMO-LUMO energy differences ( $\Delta E_{\text{H-L}}$ ); and the lowest triplet energy ( $E_{\text{T}}$ ). (d) Electrostatic potential maps of **TPy-BP** and **DPmPy-BP**.

# 2.2. Synthesis and physical properties

The synthetic route of **DPmPy-BP** is shown in Figure S5. **DPmPy-BP** could be easily prepared on the gram scale by a two-step reaction, starting with the Kröhnke-type ring-closure reaction then followed by Suzuki coupling reaction. The target compound was characterized by <sup>1</sup>H and <sup>13</sup>C nuclear magnetic resonance (NMR), mass spectrometry (Figures S6-S7), elemental analysis and purified by temperature-gradient vacuum sublimation. The molecular structures of **TPy-BP** and **DPmPy-BP** were confirmed by X-ray diffraction (XRD) analysis of the single crystals (Figures S8-S9, Table S1). The dihedral angles between two peripheral pyrimidine and core pyridine rings of **DPmPy-BP** (A'-B': 170.52°, A'-C': 171.28°) are slightly smaller than those of **TPy-BP** (A-B: 177.38°, A-C: 178.37°), suggesting quasi-planar structures of both **TPy** and **DPmPy** parts. Remarkably, the most stable conformation of **DPmPy-BP** in crystals was desirable to strengthen metal complexation as expected.

The thermal properties of **TPy-BP** and **DPmPy-BP** were investigated by thermogravimetric analysis (TGA) and differential scanning calorimetry (DSC) (Figures S10-S11 and **Table 1**). With comparable molar weight, **DPmPy-BP** exhibited a higher  $T_{d5}$  value about 375 °C. No  $T_{g}$ 

curve was detected from these two molecules. Note that two different  $T_c$  values of **TPy-BP** could be inferred from the separately conformational changes of two peripheral pyridines under heating. The  $T_m$  values increased as **TPy-BP** (199 °C) < **DPmPy-BP** (274 °C) indicating the rising intermolecular interactions in the same order as predicted. Then the photophysical properties such as ionization potential ( $I_p$ ), optical energy gap ( $E_g$ ) and  $E_T$  were investigated by using photoelectron yield spectrometry (PYS), UV-vis absorption spectra and low-temperature photoluminescence (PL) spectra in dilute 2-methyltetrahydrofuran solutions, respectively (Figures S12-S15 and Table 1). The electron affinity ( $E_a$ ) was then determined by the  $I_p$  and  $E_g$  values. **DPmPy-BP** exhibited deeper  $I_p$  value of 6.55 eV, indicating its potential usefulness as hole-blocking layer (HBL). Consistent with the DFT calculations, deeper  $E_a$  value of **DPmPy-BP** suggested that when only taking energy level into account, its electroninjection barrier from the cathode aluminum metal would be lower than **TPy-BP**. Furthermore, both **TPy-BP** and **DPmPy-BP** exhibited high  $E_T$  values of around 2.7 eV estimated from the onset of phosphorescence spectra.

Table 1. Summary of physical properties

ETM	MW	$T_g^{\rm a}/T_c^{\rm a}/T_m^{\rm a}/T_{d5}^{\rm b}$ HOMOc/LUMOc/ $E_T^{\rm d}$		$I_p^{ m e}/E_g^{ m f}/E_a^{ m g}/E_T^{ m h}$	
		[°C]	[eV]	[eV]	
ВСР	360.5	86/ 143/ 287/ 317	-5.96/ -1.46/ 2.61	6.45/ 3.65/ 2.80/ 2.6	
TPy-BP	385.5	n.d./ 108/ 199/ 327	-5.95/ -1.50/ 2.86	6.50/ 3.51/ 2.99/ 2.78	
DPmPy-BP	387.4	n.d./ n.d./ 274/ 375	-5.98/ -1.59/ 2.89	6.55/ 3.51/ 3.04/ 2.68	

a)  $T_g$ ,  $T_c$  and  $T_m$  values were confirmed by DSC. b)  $T_{d5}$  was measured using TGA. c,d) Calculated at the B3LYP/6-31G(d)// B3LYP 6-31G(d) level. d) Calculated triplet energies. e)  $I_p$  was determined by using PYS. f)  $E_g$  was estimated at the point of intersection of the UV-vis spectra, g) The value of  $E_a$  was calculated using  $I_p$  and  $E_g$ . h)  $E_T$  was determined from the onset of the phosphorescent spectra at 80 K in 2-methyltetrahydrofuran.  $E_T$  of **BCP** was reported previously. [27]

# 2.3. Electron-injection and interactions with silver

To verify the actual electron-injection barriers (EIB) from Al cathodes, the changes of vacuum levels ( $E_{\rm vac}$ ) were investigated by ultraviolet photoelectron spectroscopy (UPS) measurements on samples of [ITO/Al (20 nm)] and [ITO/Al (20 nm)/ETL: Ag (5 nm, 80 wt%: 20 wt%)] (**Figure 3**a and S19). The Ag doping concentration of 20 wt% were determined to maintain the molar ratio of ETMs:Ag over 1:1 aiming for facilitated silver complexation, while manipulated by a volume ratio of 4.88:0.12 during the film sublimation (Table S2). The  $E_{\rm vac}$ , which was obtained from the measured energy of the secondary-electron cutoff, [28] shifted down for all Ag-doped ETMs, in detail, **TPy-BP** (0.16 eV) < **BCP** (0.54 eV) < **DPmPy-BP** (0.73 eV). In comparison to their  $E_{\rm a}$  values, the Schottky type EIB from

cathodes increased with the order of **DPmPy-BP** (0.43 eV) < **BCP** (0.86 eV) < **TPy-BP** (1.05 eV) (Figure 3b). When combined with silver, **DPmPy-BP** showed better electron-injection ability than both **BCP** and **TPy-BP**, demonstrating its potential as a new Ag-partner in terms of the air-stable EIL.

To further discuss the interactions between silver and ETMs, X-ray photoelectron spectroscopy (XPS) measurements were carried out to study the chemical state of silver (Figure 3c). Interestingly, for **TPy-BP** the core level of Ag 3d nearly remained unshifted while that of **DPmPy-BP** shifted for about 0.6 eV, suggesting much stronger complexation of silver when interacted with **DPmPy-BP** than **TPy-BP**. In conformity with our design strategy and DFT calculation, this result affirmed that Ag complexation depended on the conformational isomerism of ligands. Furthermore, with all aspects considered, it possibly validated that the electron-injection of ETMs combined with Ag correlated with the conformation-dependent Ag complexation.

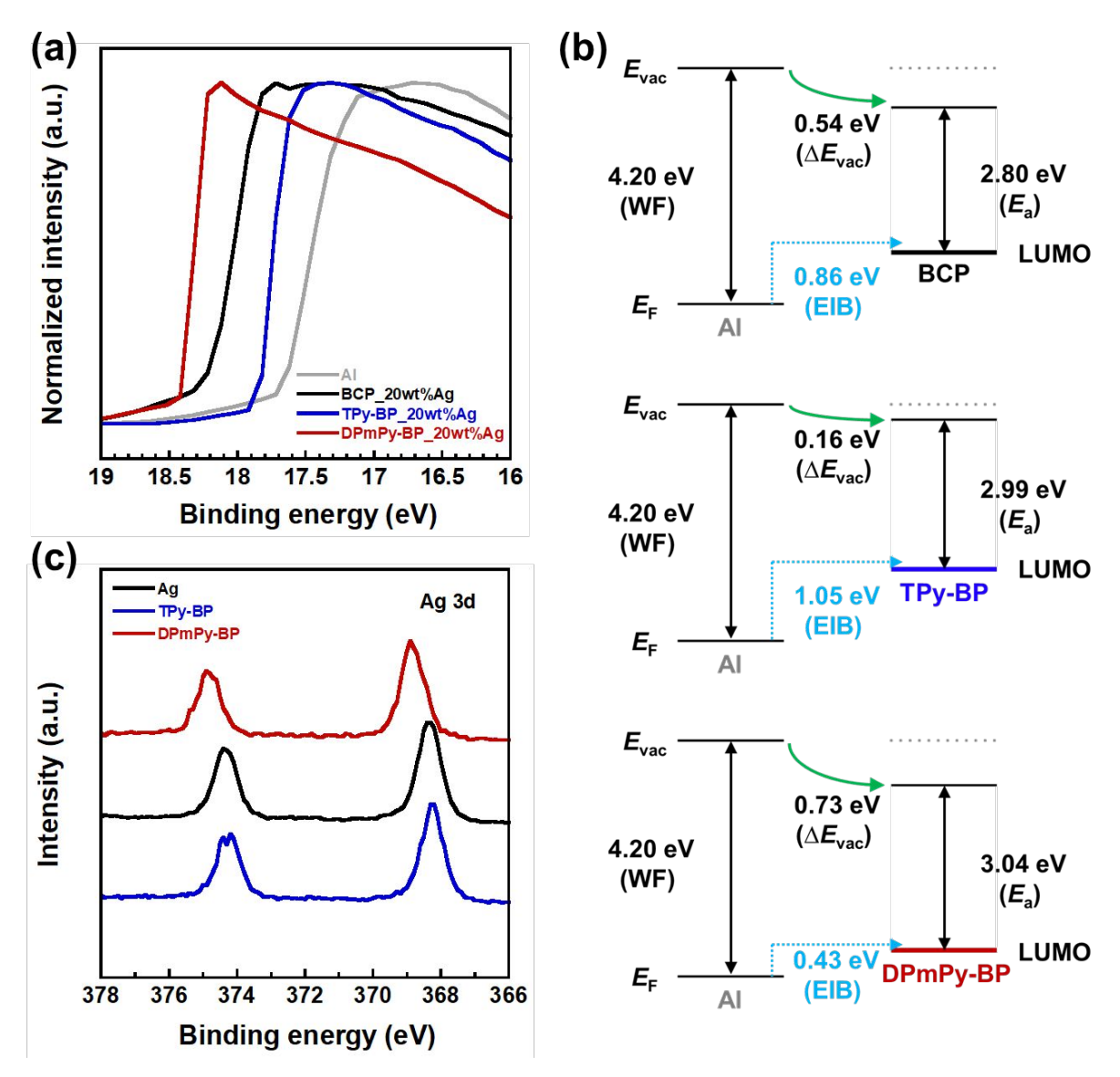


**Figure 3.** (a) UPS analysis of ITO/Al (20 nm), ITO/Al (20 nm)/ETL: Ag (5 nm, 80wt%: 20 wt%) in the secondary electron cutoff region. (b) Summary of the energy diagrams estimated by the UPS, PYS and UV-vis measurements around Al cathode where  $\Delta E_{\rm vac}$  and  $E_{\rm F}$  stand for the shift of vacuum levels and the fermi level, respectively. The WF of Al was determined based on the UPS. <sup>[29]</sup> (c) XPS analysis of ITO/Ag (20 nm), ITO/Ag (20 nm)/ETL (7 nm).

### 2.4. OLED fabrication and performance

To demonstrate the potential usefulness of **DPmPy-BP** serving as the ETL, the HBL, and as the EIL combined with silver simultaneously, conventional green phosphorescent OLEDs based on **Ir(ppy)**<sub>3</sub><sup>[30]</sup> with the structures of [ITO (100 nm)/polymer buffer<sup>[31]</sup> (20 nm)/**NPD** (10 nm)/**4DBFHPB**<sup>[32]</sup> (10 nm)/**DIC-TRZ**<sup>[33]</sup> : **Ir(ppy)**<sub>3</sub> (20 nm, 88 wt%: 12 wt%)/ETL (50 nm)/**Liq** (1 nm)/Al (100 nm)] and [ITO (100 nm)/polymer buffer (20 nm)/**NPD** (10 nm)/**4DBFHPB** (10 nm)/**DIC-TRZ** : **Ir(ppy)**<sub>3</sub> (20 nm, 88 wt%: 12 wt%)/ETL (45 nm)/ETL: Ag (5 nm, 80 wt%: 20 wt%)/Al (100 nm)] were fabricated (Figure S20). Both **BCP** (**Figure 4**, **Table 2**) and **TPy-BP** (Figures S21-26, Table S3) were compared.

The energy diagram of the device is displayed in Figure 4a and S18. As depicted in Figure 4 and summarized in Table 2, all the devices showed typical green electroluminescence (EL) from  $Ir(ppy)_3$  with a peak wavelength of 516 nm. Slight changes on the shoulder peak around 560 nm, probably attributed to the differently localized emitting center presumably due to the carrier balance in each device. For Liq-based devices, in contrast to BCP, DPmPy-BP exhibited lower current densities (J) and causally lower luminance (L) in the low voltage (V) region ( $\sim 2.4 \text{ V}$ ), attributed to a larger electron-injection barrier from DPmPy-BP to EML induced by its deeper LUMO. Impressively, with a steeper rise in the J-V characteristics of DPmPy-BP, both the turn-on voltage (V<sub>on</sub>) and the operational voltage of certain L were relatively lower than those of BCP, implying better electron transporting properties of DPmPy-BP. Due to more balanced carriers conducted by faster electrons, DPmPy-BP achieved a higher maximum EQE around 23%, better roll-off performance, and a longer lifetime ( $LT_{50}$ ) around 16 000 h with an initial luminance ( $L_0$ ) of 1 000 cd m<sup>-2</sup>.

On the other hand, for Ag-doped devices, the variety of the electron-injection properties from the cathode to ETMs demonstrated dominating impacts on the device performance. Compared ETL:Ag with **Liq** as EIL, the changes in electron-injection abilities from cathodes to ETLs resulted in changes of the carrier balances, thus EQEs changed. It is noteworthy that being comparable to its **Liq**-based device, **DPmPy-BP** combined with Ag exhibited much lower  $V_{\text{on}}$ , better J-V and V-L characteristics, as well as higher EQE in contrast to **BCP**. Especially, small inferiority on the roll-off, comparing to its **Liq**-based device, a prolonged LT<sub>50</sub> over 16 900 h at 1000 cd m<sup>-2</sup> was recorded for the **DPmPy-BP**/Ag device, surpassing that of **BCP**/Ag.

To further evaluate the electron-injection effect from the Al cathode to the ETMs, electrononly devices (EODs) with structures of ITO/ETL (60 nm)/Liq (1 nm)/Al (100 nm) and ITO/ETL (55 nm)/ETL: Ag (5 nm, 80 wt%: 20 wt%)/Al (100 nm) were fabricated, where BCP, TPy-BP and DPmPy-BP were used as ETLs. As shown in Figure S27, comparing to the Liq-based EODs of all ETMs, the J of their Ag-doped EODs are individually lower at the same V. Considering the quantification of the electron-injection performance, the J ratio of Ag-doped ETLs to Liq based on J-V of EODs was plotted versus the average applied electric field (Figure S28). Under an average electric field of 200 kV cm<sup>-1</sup>, the J ratio increased with the order of TPy-BP (0.01) < BCP (0.06) < DPmPy-BP (0.77), suggesting superior electron injection from the cathode to the ETM of **DPmPy-BP** when doped with Ag, which was consistent with both the results of UPS and the performance of devices.

Finally, to assess the air-stability, images of the unencapsulated OLEDs were with the driving voltage fixed at 7 V (Figure S29). The luminance differed due to the differences in *J-V* characteristics, with **TPy-BP/Liq** and **DPmPy-BP/Liq** having higher initial luminance but the increase of the number and the size of the dark spots and the shrinkage of the emitting area were obvious. The **BCP/Liq** and **BCP/Ag** devices were even worse, possibly due to the unstable nature of **BCP**. [6] For example, more than 100 dark spots were observed after 24 h in the **BCP/Ag** and **BCP/Liq** devices, while only several dark spots were observed in the **DPmPy-BP/Ag** device. Regarding the proliferation of black spots, area shrinkage and brightness, the **DPmPy-BP/Ag** device apparently exhibits best air stability among all conditions. These results highlighted the suitability of **DPmPy-BP** as a superior electron-transporting **Ag**-partner in terms of the air-stable EIL.

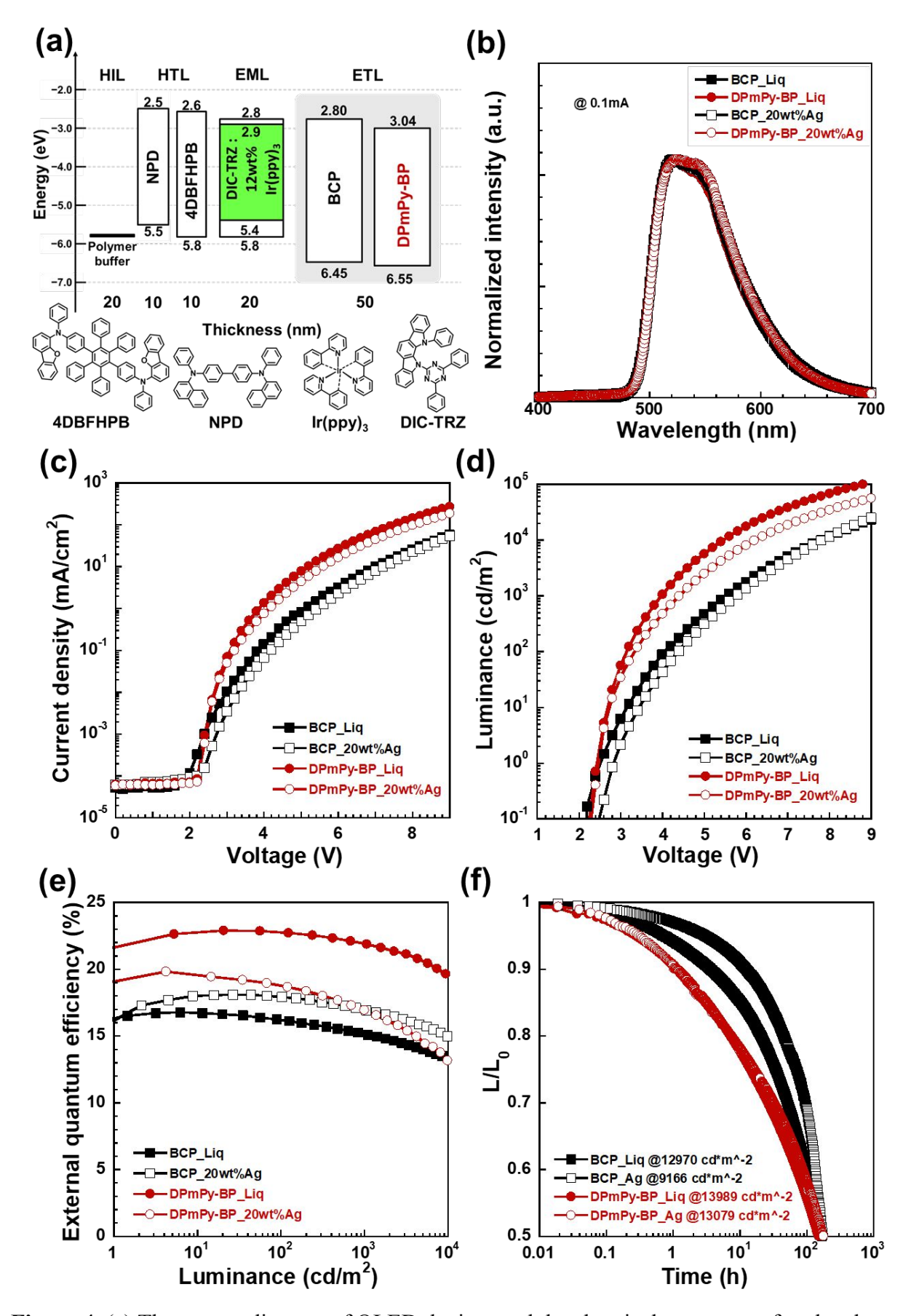


**Figure 4.** (a) The energy diagram of OLED devices and the chemical structures of molecules used. (b) Normalized EL spectra. (c, d) The current density and luminance versus voltage

characteristics. (e) EQE versus luminance characteristics. (f) Operation lifetime of encapsulated devices till 50% of initial luminance at 25 mA cm<sup>-2</sup>.

Table 2. Summary of OLED performance

electron-	ETM	$V_{ m on}{}^{ m a}$	$V_{100}/\eta_{\rm p,100}/\eta_{ m c,100}/\eta_{ m ext,100}{}^{ m b}$	$V_{1000}/\eta_{\rm p,1000}/\eta_{\rm c,1000}/\eta_{\rm ext,1000}^{ m c}$	$LT_{50}^{d}$
injection		[V]	[V/lm W <sup>-1</sup> /cd A <sup>-1</sup> /%]	[V/lm W <sup>-1</sup> /cd A <sup>-1</sup> /%]	[h]
Liq	BCP	2.49	4.10/ 45.1/ 59.2/ 16.2	5.52/ 31.7/ 55.7/ 15.7	14892
	DPmPy-BP	2.41	3.13/81.4/81.0/22.8	3.97/ 61.8/ 78.0/ 21.9	16291
ETM:Ag	BCP	2.82	4.38/ 45.9/ 64.0/ 17.9	5.76/ 33.0/ 60.6/ 17.0	8305
	DPmPy-BP	2.43	3.32/63.7/67.3/18.8	4.40/ 43.3/ 60.6/ 16.9	16913

a) Turn on voltage ( $V_{on}$ ) at 1 cd m<sup>-2</sup>. b) Voltage (V), power efficiency ( $\eta_p$ ), current efficiency ( $\eta_c$ ) and external quantum efficiency ( $\eta_{ext}$ ) at 100 cd m<sup>-2</sup>. c) V,  $\eta_p$ ,  $\eta_c$  and  $\eta_{ext}$  at 1000 cd m<sup>-2</sup>. d) Operational lifetime at 50% (LT<sub>50</sub>) at 1000 cd m<sup>-2</sup>, using the formula LT( $L_1$ ) = LT( $L_0$ ) ( $L_0/L_1$ ) <sup>n [34]</sup>, where  $L_1$  is the desired luminance while the escalation factors (n) are determined to be 1.75.

#### 3. Conclusion

As a potential air-stable EIL combined with Ag, we developed a novel non-Phen derivative named **DPmPy-BP**. Remarkably, compared with the conventional Phen-based ETM such as **BCP**, **DPmPy-BP** had deeper  $I_p$  value around 6.55 eV and  $E_a$  value of 3.04 eV, as well as higher  $E_T$  values around 2.7 eV. This ETM also exhibited much better electron-injection properties when doped with Ag probably due to the conformation-dependent metal complexation. As a proof-of-concept, the corresponding green phosphorescent OLEDs using **DPmPy-BP**/Ag achieved a lower turn-on voltage, a higher EQE, and higher operational stability compared with those based on **BCP**/Ag. These performances were also comparable to those based on the conventional alkali metal compound **Liq** as the EIL (**DPmPy-BP/Liq**). Consequently, we propose **DPmPy** derivatives as promising candidates for advanced ETMs, given high  $E_T$ , superior electron-injection with silver, and enhanced potential for chemical modifications. We believe that our work would inspire the development of new materials and illuminate the path toward next generation OLED industry.

#### **Conflicts of interest**

There are no conflicts to declare.

#### Acknowledgements

We gratefully acknowledge the subsidy program for the development of advanced research infrastructure from the Ministry of Education, Culture, Sports, Science, and Technology

(MEXT). T. S., H. S. and J. K. acknowledges the partial financial support provided by the Strategic International Collaborative Research Program (SICORP) from the Japan Science and Technology Agency (JST) (JPMJSC2007). H. S. acknowledges the partial financial support provided by JSPS KAKENHI (23H02032 and 23K26725).

#### References

- [1] a) H. Sasabe, J. Kido, *Eur. J. Org. Chem.* **2013**, 7653-7663; b) S. Izawa, M. Morimoto, K. Fujimoto, K. Banno, Y. Majima, M. Takahashi, S. Naka, M. Hiramoto, *Nat. Commun.* **2023**, 14, 5494.
- [2] L. S. Hung, C. W. Tang, M. G. Mason, Appl. Phys. Lett. 1997, 70, 152-154.
- [3] J. Kido, T. Matsumoto, Appl. Phys. Lett. 1998, 73, 20, 2866-2868.
- [4] G. Parthasarathy, C. Shen, A. Kahn, S. R. Forrest, *J. Appl. Phys.* **2001**, 89, 4986-4992.
- [5] J. Endo, T. Matsumoto, J. Kido, Jpn. J. Appl. Phys. 2002, 41, L800-L803.
- [6] S. Scholz, D. Kondakov, B. Lüssem, K. Leo, *Chem. Rev.* **2015**, 115, 16, 8449-8503.
- [7] Y. Zhou, C. Fuentes-Hernandez, J. Shim, J. Meyer, A. J. Giordano, H. Li, P.Winget, T. Papadopoulos, H. Cheun, J. Kim, M. Fenoll, A. Dindar, W. Haske, E. Najafabadi, T. M. Khan, H. Sojoudi, S. Barlow, S. Graham, J. Brédas, S. R. Marder, A. Kahn, and B. Kippelen. *Science* **2012**, 336, 327-332.
- [8] H. Lee, G. Cho, S. Woo, S. Nam, J. Jeong, H. Kim, Y. Kim, *RSC Adv.* **2012**, 2, 8762-8767.
- [9] S. Sato, S. Ohisa, Y. Hayashi, R. Sato, D. Yokoyama, T. Kato, M. Suzuki, T. Chiba, Y.-J. Pu, J. Kido, *Adv. Mater.* **2018**, 30, 1705915.
- [10] T. Sasaki, M. Hasegawa, K. Inagaki, H. Ito, K. Suzuki, T. Oono, K. Morii, T. Shimizu, H. Fukagawa, *Nat. Commun.* **2021**, 12, 2706.
- [11] T. Sakurai, S. Toyoshima, H. Kitazume, S. Masuda, H. Kato, K. Akimoto, *J. Appl. Phys.* **2010**, 107, 043707.
- [12] F. Yan, X. W. Sun, Appl. Phys. Lett. 2013, 102, 043303.
- [13] H. Yoshida, J. Phys. Chem. C 2015, 119, 24459-24464.
- [14] Z. Bin, G. Dong, P. Wei, Z. Liu, D. Zhang, R. Su, Y. Qiu, L. Duan, *Nat. Commun.* **2019**, 10, 866.
- [15] Y. Chen, X. Liu, S. Braun, Y. Wang, M. Fahlman, *J. Mater. Chem. C* **2020**, 8, 173-179.
- [16] H. Fukagawa, K. Suzuki, H. Ito, K. Inagaki, T. Sasaki, T. Oono, M. Hasegawa, K. Morii, T. Shimizu, *Nat. Commun.* **2020**, 11, 3700.

- [17] a) G. W. Kim, Y. H. Son, H. I. Yang, J. H. Park, I. J. Ko, R. Lampande, J. Sakong, M. -J. Maeng, J. -A. Hong, J. Y. Lee, Y. Park, J. H. Kwon, *Chem. Mater.* 2017, 29 (19), 8299-8312; b) S. K. Kim, R. Lampande, J. H. Kwon, *ACS Photonics* 2019, 6 (11), 2957-2965.
- [18] Z. Bin, D. Shi, R. Su, W. Han, D. Zhang, L. Duan, Sci. Bull. 2020, 65, 153-160.
- [19] Z. Liu, X. Li, Y. Lu, C. Zhang, Y. Zhang, T. Huang, D. Zhang, L. Duan, *Nat. Commun.* **2022**, 13, 1215.
- [20] N. Notsuka, R. Kabe, K. Goushi, C. Adachi, Adv. Funct. Mater. 2017, 27, 1703902.
- [21] Y. Shi, Z. Bin, J. Liu, W. Han, G. Yang, B. Lei, J. You, *Angew. Chem. Int. Ed.* **2022**, 61, e202202898.
- [22] Y. Liu, J. Guo, R. Liu, Q. Wang, X. Jin, L. Ma, W. Lv, S. Liu, S. Yuan, H. Zhu, *J. Lumin.* **2015**, 157, 249-256.
- [23] a) E. C. Constable *Chem. Soc. Rev.* **2007**, 36, 246-253; b) A. Wild, A. Winter, F. Schlütter, U. S. Schubert, *Chem. Soc. Rev.* **2011**, 40, 1459-1511; c) G. R. Whittell, M. D. Hager, U. S. Schubert and I. Manners, *Nat. Mater.* **2011**, 10, 176-188.
- [24] a) Y. Watanabe, R. Yoshioka, H. Sasabe, T. Kamata, H. Katagiri, D. Yokoyama, J. Kido, *J. Mater. Chem. C* **2016**, 4, 8980; b) Y. Watanabe, D. Yokoyama, T. Koganezawa, H. Katagiri, T. Ito, S. Ohisa, T. Chiba, H. Sasabe, J. Kido, *Adv. Mater.* **2019**, 31, 1808300; c) T. Maruyama, H. Sasabe, Y. Watanabe, T. Owada, R. Yoshioka, Y. Saito, T. Kawano and J. Kido, *Chem. Lett.* **2021**, 50, 534.
- [25] R.-J. Chein and E. J. Corey, *Org. Lett.* **2010**, 12 (1), 132-135.
- [26] *Gaussian 09*, Revision D.01, M. J. Frisch, G. W. Trucks, H. B. Schlegel, G. E. Scuseria, M. A. Robb, J. R. Cheeseman, G. Scalmani, V. Barone, B. Mennucci, G. A. Petersson, H. Nakatsuji, M. Caricato, X. Li, H. P. Hratchian, A. F. Izmaylov, J. Bloino, G. Zheng, J. L. Sonnenberg, M. Hada, M. Ehara, K. Toyota, R. Fukuda, J. Hasegawa, M. Ishida, T. Nakajima, Y. Honda, O. Kitao, H. Nakai, T. Vreven, J. A. Montgomery, Jr., J. E. Peralta, F. Ogliaro, M. Bearpark, J. J. Heyd, E. Brothers, K. N. Kudin, V. N. Staroverov, R. Kobayashi, J. Normand, K. Raghavachari, A. Rendell, J. C. Burant, S. S. Iyengar, J. Tomasi, M. Cossi, N. Rega, J. M. Millam, M. Klene, J. E. Knox, J. B. Cross, V. Bakken, C. Adamo, J. Jaramillo, R. Gomperts, R. E. Stratmann, O. Yazyev, A. J. Austin, R. Cammi, C. Pomelli, J. W. Ochterski, R. L. Martin, K. Morokuma, V. G. Zakrzewski, G. A. Voth, P. Salvador, J. J. Dannenberg, S. Dapprich, A. D. Daniels, Ö. Farkas, J. B. Foresman, J. V. Ortiz, J. Cioslowski, and D. J. Fox, Gaussian, Inc., Wallingford CT, 2013.
- [27] T. Xu, Y.-X. Zhang, B. Wang, C.-C. Huang, I. Murtaza, H. Meng, L. S. Liao, *ACS Appl. Mater. Interfaces.* **2017**, 9 (3), 2701-2710.

- [28] H. Ishii, K. Sugiyama, E. Ito, K. Seki, Adv. Mater. 1999, 11, 605.
- [29] D. Cahen, A. Kahn, Adv. Mater. 2003, 15, 271-277.
- [30] S. Lamansky, P. Djurovich, D. Murphy, F. Abdel-Razzaq, R. Kwong, I. Tsyba, M.
- Bortz, B. Mui, R. Bau, M. E. Thompson, Inorg. Chem. 2001, 40 (7), 1704-1711.
- [31] J. Kido, G. Harada, M. Komada, H. Shionoya, K. Nagai, *ACS Symp. Ser.* **1997**, 672, 381.
- [32] a) T. Kamata, H. Sasabe, M. Igarashi, J. Kido, *Chem. Eur. J.* **2018**, 24, 4590; b) T. Kamata, H. Sasabe, N. Ito, Y. Sukegawa, A. Arai, T. Chiba, D. Yokoyama, J. Kido, *J. Mater. Chem. C* **2020**, 8, 7200.
- [33] D. Zhang, L. Duan, C. Li, Y. Li, H. Li, D. Zhang, Y. Qiu, Adv. Mater. 2014, 26, 5050.
- [34] C. Féry, B. Racine, D. Vaufrey, H. Doyeux, S. Cinà, *Appl. Phys. Lett.* **2005**, 87 (21), 213502.

# Data availability statements

- The data supporting this article have been included as part of the Supplementary Information.
- Crystallographic data for TPy-BP and DPmPy-BP have been deposited at Cambridge Crystallographic Data Centre (CCDC) under [CCDC 2378345-2378346].